Evaluation of sibling and twin fragment ions improves the structural characterization of proteins by top-down MALDI in-source decay mass spectrometry

Nicolardi, S.; Kilgour, D.P.A.; Dolezal, N.; Drijfhout, J.W.; Wuhrer, M.; Burgt, Y.E.M. van der

Evaluation of Sibling and Twin Fragment Ions Improves the Structural Characterization of Proteins by Top-Down MALDI In-Source Decay Mass Spectrometry

Simone Nicolardi,* David P. A. Kilgour, Natasja Dolezal, Jan W. Drijfhout, Manfred Wuhrer, and Yuri E. M. van der Burgt

Read Online

ACCESS | Metrics & More | Article Recommendations | SI Supporting Information

ABSTRACT: Comprehensive determination of primary sequence and identification of post-translational modifications (PTMs) are key elements in protein structural analysis. Various mass spectrometry (MS) based fragmentation techniques are powerful approaches for mapping both the amino acid sequence and PTMs; one of these techniques is matrix-assisted laser desorption/ionization (MALDI), combined with in-source decay (ISD) fragmentation and Fourier-transform ion cyclotron resonance (FT-ICR) MS. MALDI-ISD MS protein analysis involves only minimal sample preparation and does not require spectral deconvolution. The resulting MALDI-ISD MS data is complementary to electrospray ionization-based MS/MS sequencing readouts, providing knowledge on the types of fragment ions is available. In this study, we evaluate the isotopic distributions of z' ions in protein top-down MALDI-ISD FT-ICR mass spectra and show why these distributions can deviate from theoretical profiles as a result of co-occurring and isomeric z and y-NH$_3$ ions. Two synthetic peptides, containing either normal or deuterated alanine residues, were used to confirm the presence and unravel the identity of isomeric z and y-NH$_3$ fragment ions ("twins"). Furthermore, two reducing MALDI matrices, namely 1,5-diaminonaphthalene and N-phenyl-p-phenylenediamine were applied that yield ISD mass spectra with different fragment ion distributions. This study demonstrates that the relative abundance of isomeric z and y-NH$_3$ ions requires consideration for accurate and confident assignments of z' ions in MALDI-ISD FT-ICR mass spectra.
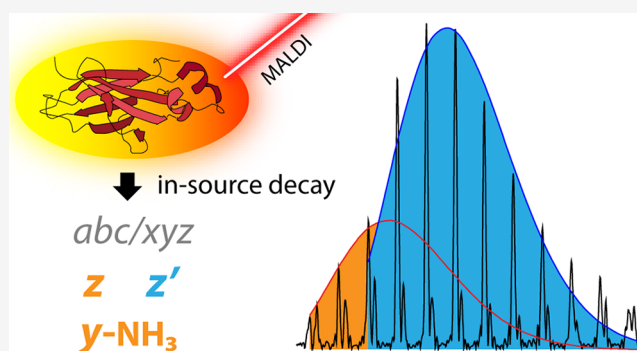
Mass spectrometry (MS) is a core technology for the structural characterization of peptides and proteins. MS analysis of proteins commonly involves the determination of the primary structure and any post-translational modifications (PTMs), by applying diverse fragmentation strategies that provide complementary sequence information.[1−9] In general, after ion activation in the gas phase, cleavage of a peptide bond occurs at the weaker amide bond, the adjacent C−C bond, or the N−Cα bond, in a process commonly referred to as *abc−xyz* fragmentation (Figure S1).[10−14] Secondary fragmentation reactions can occur, mostly involving the loss of neutrals such as water and ammonia.[15,16] In radical-mediated fragmentation, different types of ions are formed as a result of the loss of amino acid side chains.

A clear understanding of fragmentation pathways is essential for an accurate interpretation of MS spectra and to allow confident structural analysis of peptides and proteins. In general, collision-induced dissociation (CID) and higher-energy collisional dissociation (HCD) lead to the formation of *b* and *y* ions; electron transfer dissociation (ETD) and electron capture dissociation (ECD) lead to the formation of *c*-

and *z*-types;[3,8,17−20] and ultraviolet photodissociation (UVPD) results in a plethora of fragment ions.[21−23] Mixed mode techniques, such as electron transfer HCD or activated-ion ETD, are used to increase the number of fragmentation pathways, aiming for extended protein sequence coverage.[24] It is noted that these fragmentation techniques are often applied for the characterization of multiply charged proteins generated by electrospray ionization (ESI) where fragment ions appear in different charge states. As a result, ESI protein fragmentation spectra are complex and often include overlapping signals from fragment ions with different charges.[25]

In contrast, matrix-assisted laser desorption ionization (MALDI) predominantly yields singly charged ions.[26−28]
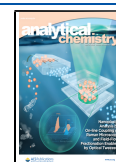
The use of specific MALDI matrices, in combination with high laser fluence, allows protein fragmentation in a process referred to as "in-source decay" (ISD).[28,29] Despite the fact that lower charge state ions are more difficult to fragment than multiply charged ones, MALDI-ISD mass spectra provide a wide range of fragment ions, distributed over a large m/z window.[27,30] Notably, in MALDI-ISD MS analysis of proteins, the protein sequence tends to be comprehensively covered over a wide m/z range that displays a continuous series of fragment ions. In addition, MALDI-ISD MS is rather tolerant to salts in the sample, requires minimal sample preparation, and is suitable for high-throughput and automated measurements.

Different compounds can be applied as a matrix in MALDI-ISD MS, each with its own characteristics and distinctive fragment ions.[30−33] Reducing matrices, such as 1,5-diaminonaphtalene (1,5-DAN), are particularly useful for the analysis of disulfide bond-containing proteins.[34,35] Their capacity to act as a hydrogen donor allows reduction of cysteine disulfide bonds and subsequent formation of an unstable radical ion that undergoes ISD. MALDI-ISD MS spectra contain a, b, c, d, w, y, and z type fragment ions.[31,36−41] As a result of the radical fragmentation mechanism, matrix-adducted z ions can also be observed and can be used for diagnostic purposes.[37] Neutral losses, for example of ammonia and water, further increase the complexity of such spectra. This large variety in fragment ions complicates or even hampers assignments in MALDI-ISD recorded at low resolving powers. In contrast, application of ultrahigh resolution instrumentation, such as Fourier transform ion cyclotron resonance (FT-ICR) and Orbitrap analyzers, allows confident identification of the fragment ions and largely alleviates the limitations regarding the complexity of MALDI-ISD spectra, as we recently demonstrated for (bivalent) monoclonal antibodies (mAbs) and functionalized nanomaterials.[38,39,42−44]

Identification of fragment ions in ultrahigh resolution MALDI-ISD spectra is based on both the m/z values and their match with theoretical isotopic distributions. Peak assignment includes consideration of the relative intensities of the different isotopologues within a certain mass error. Large deviations from the theoretical isotopic distributions could thus result in reduced confidence in automated assignments that can also cause concern during manual (visual) interpretation. Confidence in the fragment ion assignments increases upon improved matches of isotopic distributions.[45−49]

Spectral interpretation turns more complex in situations where multiple isotopic distributions from different types of fragment ions overlap. In radical-mediated fragmentation in MALDI-ISD, (sibling) ions are formed by a hydrogen addition (z') or abstraction (z) from radical z ions ($z^{•}$).[28,32,50−54] In addition, loss of ammonia from y ions results in an ion species (y-NH$_3$) isomeric with z ions (twins). The isotopic distribution of these twin ions overlaps with isotopologues from z' ions. Differentiation between these fragment ions is particularly relevant in studies where z-type ions are correlated to structural characteristics of the analyzed peptides or proteins.[50,55−58]

In this study, we evaluate the interference of the isomeric z and y-NH$_3$ ions with the signals from z' ions and demonstrate the resulting changes in the apparent relative intensity of z' ion isotopologues. This information is intended to help other researchers understand why their z' ion isotopic distributions may often deviate from the theoretical and may therefore allow more confident assignment of these fragments in spectra.

Fragment assignments in MALDI-ISD FT-ICR MS-data from insulin exemplify the importance of distinguishing various fragmentation pathways. The formation of either z or y-NH$_3$ ions is further investigated by stable isotope labeling. The importance of co-occurring z and y-NH$_3$ fragment ions will be discussed with regard to accurate assignment of z' ions in intact protein MALDI-ISD spectra.

■ MATERIAL AND METHODS

Chemicals. Human insulin, myoglobin from equine skeletal muscle, 1,5-diaminonaphtalene (1,5-DAN; handle with care, check material safety data sheet), N-phenyl-p-phenylenediamine (PPDA; handle with care, check material safety data sheet), sinapinic acid (SA), and acetonitrile (ACN; MS grade) were purchased from Sigma-Aldrich. Trifluoroacetic acid (TFA) was purchased from Thermo Fisher Scientific. Formic acid (FA) was purchased from Honeywell. Ultrapure water (Milli-Q; Merck) was used throughout this study. 2-Propanol was purchased from Biosolve BV. NIST mAb standard (HzIgG1-kappa, NS0) was provided by the Consortium for Top-Down Proteomics (CTDP).[39,59]

A 5 mg/mL solution of human insulin was prepared in water/TFA, 99.95%:0.05%. A 2 mg/mL solution of myoglobin was prepared in water. NIST mAb standard was diluted from an initial concentration of 10 mg/mL to a final concentration of 2 mg/mL using water. A saturated solution of 1,5-DAN was prepared in water/ACN/FA, 50%:49.95%:0.05%. A saturated solution of PPDA was prepared in water/2-propanol/TFA, 50%:49.95%:0.05%. A 10 mg/mL solution of SA was prepared in water/ACN, 50%:50%. MALDI matrices were freshly prepared prior to the analysis.

Synthetic Peptides. Synthetic peptides, of specific size suitable for MALDI-ISD, were prepared by solid-phase peptide synthesis on preloaded Tentagel resins using an Fmoc protocol, as has been described previously.[60] Quality control on structure and purity was performed using UPLC and MALDI time-of-flight (TOF) MS. Peptides were stored as a lyophilized powder at −20 °C until use. A 1.2 mg/mL solution of each synthetic peptide was prepared in water. Then 2 μL of each solution was diluted with 8 μL of water and processed using SPE-tips (ZipTip; Merck Millipore) filled with 0.6 μL of C18 resin. Each tip was flushed three times with 15 μL of a solution of water/ACN/FA (50%:49.9%:0.1%) and equilibrated by flushing three times with 15 μL of water. Then, 10 μL of synthetic peptide solution (at 0.24 mg/mL) was allowed to bind to the SPE-tip by pipetting 20 times in and out. Finally, the loaded SPE-tip was flushed three times with 15 μL of water and the sample was eluted in 3 μL of water/ACN/FA, 90%:9.99%:0.01%.

MALDI Spotting. For MALDI-(ISD) measurements, 1 μL of protein standard (either myoglobin, NIST mAb or insulin) was spotted onto a ground steel MALDI target plate and mixed with 1 μL of 1,5-DAN solution. The droplet was allowed to dry at room temperature. A total of 1 μL of insulin solution was also mixed with 1 μL of SA. For MALDI analysis with PPDA, 2 μL of insulin solution was spotted with 1 μL of MALDI matrix. The same matrix-to-sample ratios were used for the analysis of the synthetic peptides using 1,5-DAN and PPDA.

MALDI Mass Spectrometry. All MS measurements were performed as previously reported.[39] Briefly, MALDI-(ISD) FT-ICR MS measurements were carried out on a 15 T solariX XR
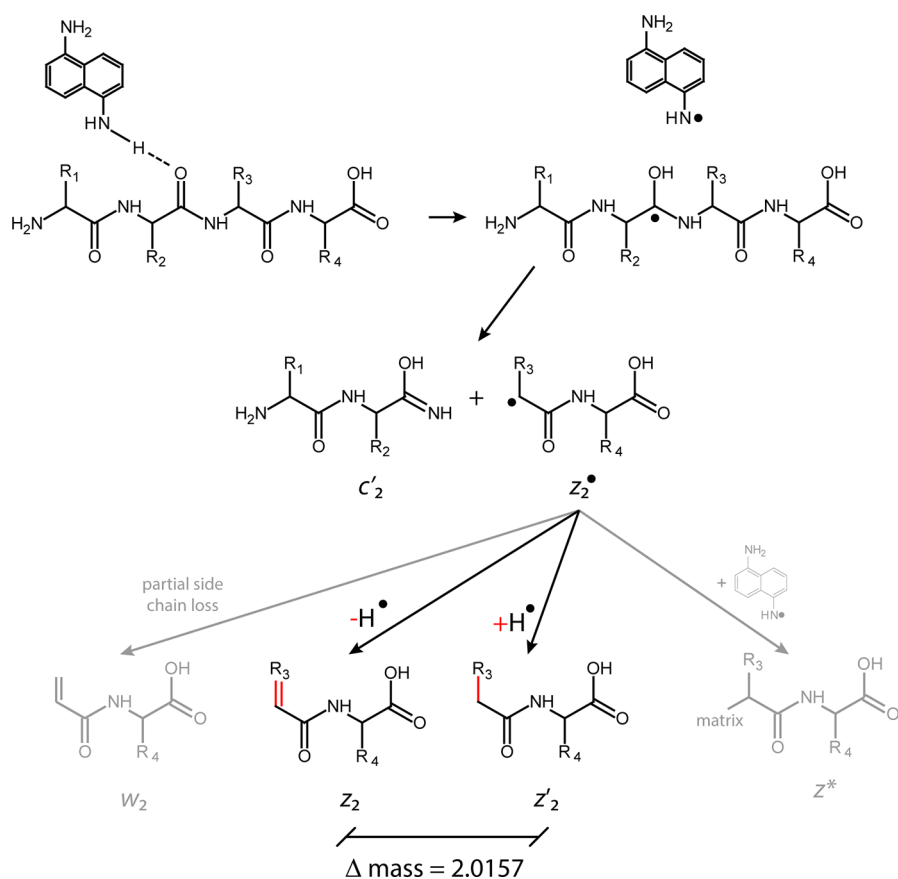
Figure 1. Radical-mediated fragmentation induced by a hydrogen-donor matrix (e.g., 1,5-DAN) in MALDI-ISD MS. Radical z ($z\bullet$) ions can further fragment into w ion or either acquire one hydrogen (from the matrix) to form z' ions or lose one hydrogen (to the radical matrix) to form z ions which have a double bond between the alpha and the beta carbon. Radical z ions can form adducts with radical matrix molecules to yield matrix-adducted z ions (z^*).

FT-ICR mass spectrometer (Bruker Daltonics) equipped with a CombiSource and a ParaCell. The MS system was controlled using ftmsControl software (Bruker Daltonics) and operated in MALDI-mode using a Smartbeam-II laser system (Bruker Daltonics), at a frequency of 500 Hz with 200 laser shots per measurement. MALDI-ISD FT-ICR MS spectra of human insulin and the synthetic peptides were acquired in the m/z ranges 1012–5000 and 1012–7000. MALDI FT-ICR MS spectra of human insulin were acquired in the m/z range 1012–7000, while MALDI FT-ICR MS spectra of the synthetic peptides were acquired in the m/z range 1012–5000. All MS spectra were acquired with 1 000 000 data points, and all data files were recorded to include the transient data (fid) file.

MALDI measurements of insulin using SA, 1,5-DAN, and PPDA were performed with a laser power of 20, 11, and 25, respectively. MALDI-ISD measurements of insulin were performed with a laser power of 20 and 30 for 1,5-DAN and PPDA, respectively, while the laser power was set to 17 and 25 for the analysis of the synthetic peptides using 1,5-DAN and PPDA, respectively. External calibration of MALDI-(ISD) FT-ICR MS acquisition methods was performed using ISD c' fragments of myoglobin.

Calculation of Theoretical Isotopic Distributions of z/y-NH$_3$ and z' Ions. A previously described, MALDI-ISD FT-ICR mass spectra of the NIST mAb were processed in both magnitude and absorption modes,[39,61−63] using AutoVectis (Spectroswiss, Lausanne, Switzerland). The peaks in both modes were detected using the AutoPiquer method,[64] in AutoVectis. The software also calculates the peak resolutions (peak m/z divided by peak full width at half the maximum intensity) and fits the appropriate best-fit curve to the combined m/z/resolution data, weighted by the peak intensity, across the mass range. For FTICR, this curve has the form

$$R = am^p + c$$

where m is the m/z of the peak and a, p, and c are coefficients that are the result of the fitting process. For FT-ICR data, the power (p) value would be expected to be close to −1 and the offset (c) to be zero. By fitting this curve to the peak lists derived from processing the same spectrum in both magnitude and absorption modes, it is possible to predict the resolution for an ion of any m/z in either mode. The resulting curves are shown in Figure S2.

Using the predictions of the resolution in both modes, the theoretical isotopic distribution of z/y-NH$_3$ and z' ions was generated using the Mercury algorithm,[65,66] for magnitude mode peaks, and a previously described method,[67] for absorption mode peaks.

Isotopic Distribution Fidelity Figure of Merit (FoM). Having generated a theoretical isotopic distribution, at the appropriate resolution and using the correct peak shape, we can calculate a figure-of-merit (FoM) to provide a measure of how closely an isotopic peak distribution in a mass spectrum matches the theoretical distribution. We investigated several different methods of producing this FoM, but found that a
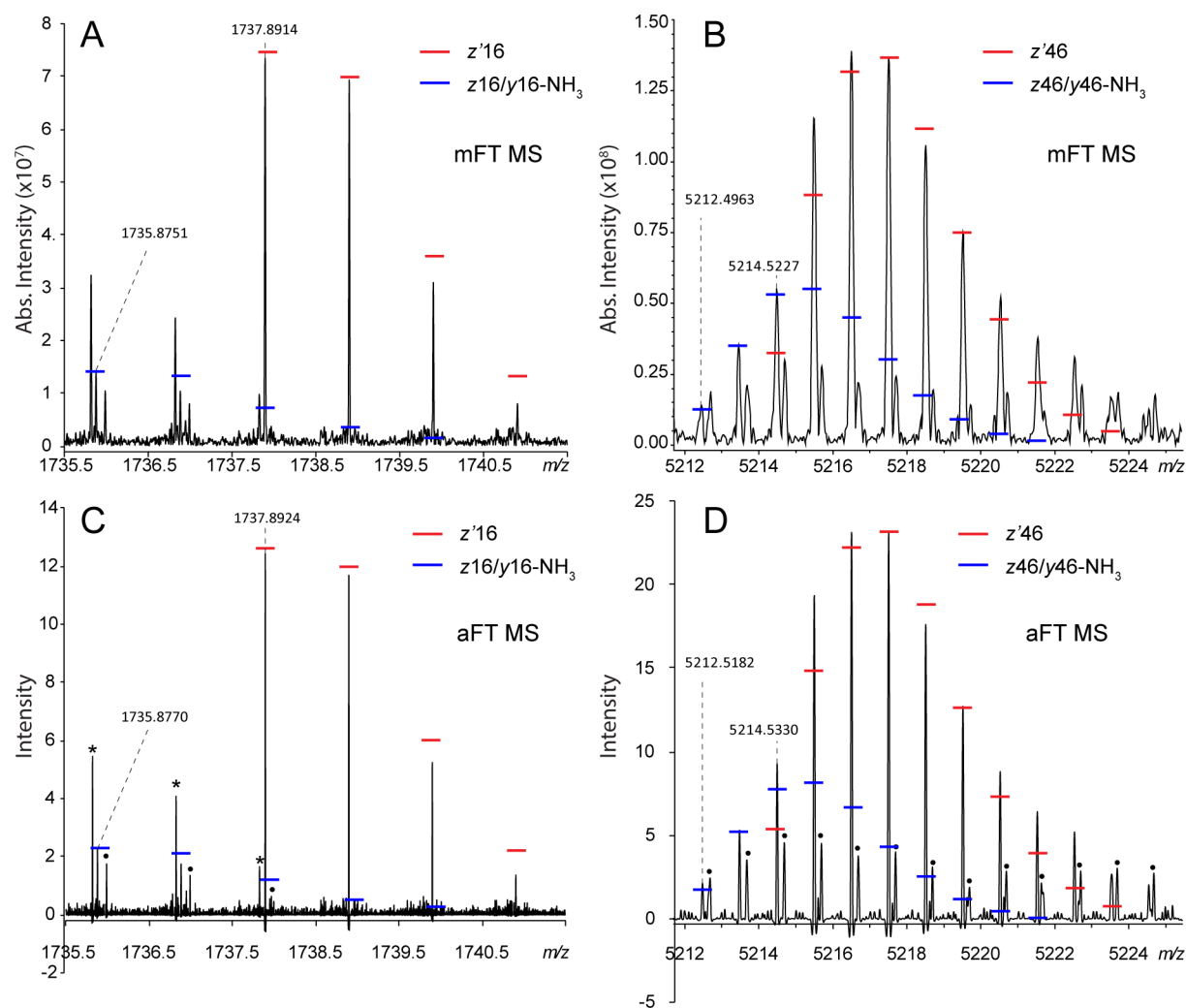
Figure 2. Isotopic distributions of z' and z/y-NH_3 ions detected in mFT (A and B) and aFT (C and D) MALDI-ISD FT-ICR MS spectra of the heavy chain of NIST mAb. The colored marks indicate the expected intensities of the fragment ion isotopologues according to theoretical isotopic distributions of z/y-NH_3 (blue) and z' (red) ions. The theoretical m/z values of $z'16$ and $z16/y16$-NH_3 are 1737.8919 and 1735.8762, respectively. The theoretical m/z-values of $z'46$ and $z46/y46$-NH_3 of the mAb heavy chain are 5214.5200 and 5212.5044, respectively. The FoM values obtained for aFT isotopic distributions of $z'16$ and $z'46$ ions were 0.95 and 0.81, respectively. * b17 of NIST mAb light chain. ● unidentified species.

simple Euclidean distance measure proved the most useful. To calculate this measure we will have a set of N spectral peaks (n = 1 to N) that we have assigned to N theoretical isotopologues. The FoM can be calculated as

$$FoM = 1 - \frac{\sqrt{\sum_{n=1}^{N}(S_n - T_n)^2}}{\sqrt{\sum_{n=1}^{N}(T_n)^2}}$$

where S_n and T_n are the normalized peak intensities of the spectral and corresponding theoretical isotopologue distributions, respectively. When the distributions match exactly, the FoM will be 1. As the distribution in the spectrum deviates from the theoretical distribution, the FoM will decrease.

We used the standard functions in AutoVectis for the generation of the mFT and aFT theoretical isotopic distributions and for the calculation of the FOMs associated with the assignments.

Data Processing. MALDI-(ISD) FT-ICR MS spectra were visualized using DataAnalysis 5.0 SR1 (Bruker Daltonics). Each MALDI-ISD FT-ICR MS spectrum was internally

calibrated using y fragments of either insulin β chain or of the synthetic peptides. Theoretical m/z values of ISD fragments were obtained using the online tool MS-Product (http://prospector.ucsf.edu/prospector/cgi-bin/msform.cgi?form=msproduct).

Absorption mode MALDI-ISD FT-ICR mass spectra were generated, processed and automatically assigned, directly from the transient data files, using the AutoVectis software suite (Spectroswiss, Lausanne, Switzerland), as previously reported.[39,61] Calibrated aFT mass spectra were exported in the "comma-separated value" (csv) format, copied in a text file and visually inspected in mMass.[68] Chemical structures were drawn in ACD/ChemSketch (Freeware) 2015. Plots were generated in Excel 2016 and figures were made in Adobe Illustrator CC 2018.

■ RESULTS AND DISCUSSION

Formation of z and z' Ions in MALDI-ISD. The previously proposed mechanism of MALDI-ISD fragmentation, using a hydrogen donor matrix, starts with the transfer of
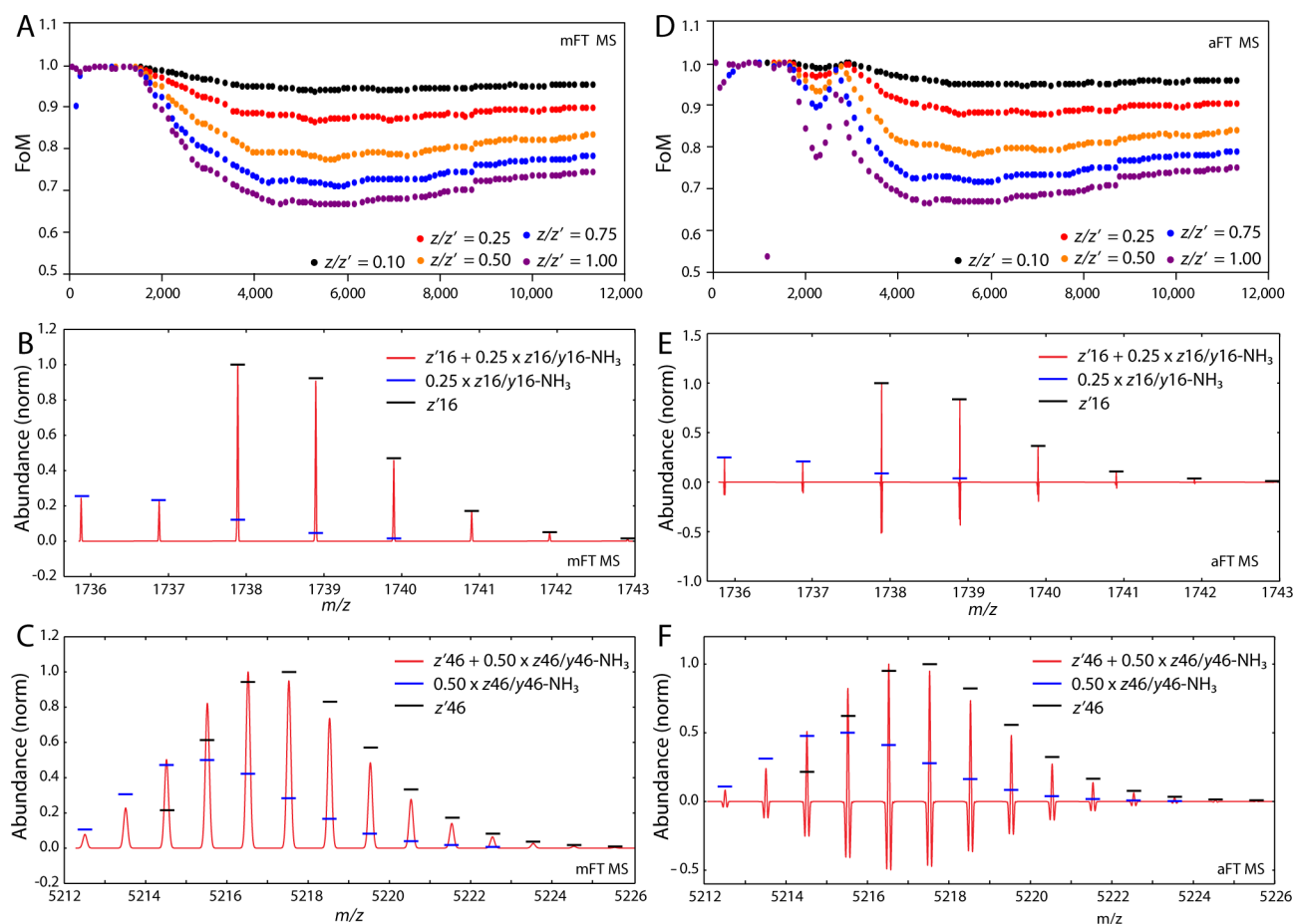
Figure 3. Evaluation of the apparent distortions of the isotopic distribution of z' ions induced by isomeric z and y-NH$_3$ ions on theoretical MALDI-ISD FT-ICR mass spectra of the heavy chain of NIST mAb. The goodness of the isotopic distribution of each z' ions, expressed as figure-of-merit (FoM) was calculated considering different z/y-NH$_3$-to-z' ratios for (A) magnitude mode (mFT) and (D) absorption mode (aFT) isotopic distributions. FoM values lower than 1 indicate a deviation of the isotopic distributions induced by the presence of z/y-NH$_3$ ions. Initially ($m/z <$ 1750), z/y-NH$_3$ and z' ions were fully resolved and theoretical distributions were observed. The decrease of resolving power along the m/z-range had the effect of inducing an overlap between z/y-NH$_3$ and z' ions which led to a distortion of the isotopic distributions as exemplified for $z'16$ and $z'46$ ion (see also Figure 2, S4, and S5) in both (B and C) mFT and aFT (E and F) distributions. The presence of z/y-NH$_3$ not only induced a change of the peak intensities of z' isotopologues but also a shift in m/z values with a consequent decrease in the mass accuracy (Figures S4−S7). The large deviations observed for aFT distributions were induced by the overlap between the negative lobes of z/y-NH$_3$ ions and the positive signal of z' ions (Figure S7). After reaching a minimum, the apparent quality of the isotopic distribution increases as a consequence of a further decrease of the resolving power and the fact that the isotopic distributions became wider and more symmetric (Figure S6).

one hydrogen atom from an amino group onto a carbonyl group (Figure 1).[54] The radical species that is obtained then fragments at the N−Cα bond resulting in radical z ($z\bullet$; "z-dot") fragments. Attachment of an additional hydrogen atom to a $z\bullet$ ion leads to the formation of the corresponding z' ion, whereas detachment of a hydrogen atom from a $z\bullet$ ion yields to the corresponding z ion. The monoisotopic ion of this latter class is detected 2.0157 mass units lower than the z' analogue, but from the third isotopologue of the z distribution, peak overlap can occur with z'.

It should be noted that $z\bullet$ ions can also further fragment and yield w ions or can form adducts with radical matrix molecules and yield matrix-adducted z ions, and these additional types of ions will also be detectable in the resulting MALDI-ISD spectra.

In addition, b and y ions are also generated in MALDI-ISD, and these ions may lose neutrals including water and ammonia. It has been previously shown by Asakawa and co-workers that the use of an intermediate-pressure MALDI source results in collisional activation of peptides and protein early in the

desorption process. Such early collisional activation can lead to a and y fragment ions via the formation of the $a\bullet/x'$ fragment pair.[41,69] As for other collision-based fragmentation techniques, this activation process can promote the loss of neutrals. For arginine, lysine, glutamate, and asparagine residues, the losses of ammonia from y ions (i.e., y-NH$_3$) are common, resulting in fragments that are isomeric with z ions (i.e., have the same elemental formulas and hence are completely isobaric). Consequently, we will refer to these isomeric, twin ions as z/y-NH$_3$.

Overlap of z/y-NH$_3$ and z' Ions in Top-Down MALDI-ISD FT-ICR Protein Spectra. In our previous MALDI-ISD studies, for simplicity reasons, only z' ions (also referred to as z + 1 ions) were assigned in top-down mass spectra since these were more intense than z/y-NH$_3$ ions.[38,39,42,70] However, especially for larger fragments, deviations from theoretical isotopic distributions revealed peak overlap of the isotopologues of the z' ions with the z/y-NH$_3$ ion isotopic distributions. This is illustrated in Figure 2, with the observed and theoretical isotopic distributions of the $z'16$ and $z16/y16$-

Figure 4. Evaluation of isomeric z and y-NH$_3$ fragment ions in MALDI-ISD FT-ICR MS spectra of human insulin analyzed using (A) 1,5-DAN and (B) PPDA as MALDI matrices. The full mass spectra are reported in Figures S12−S14. The two MALDI matrices led to similar fragmentation profiles with differences observed for the ratio between z/y-NH3 and z' ions, Y and y, and b and d. In addition, PPDA led to a less efficient reduction of the intrachain disulfide bond of insulin α-chain c' fragments. (C) Chemical structures of C-terminal fragment ions generated from the cleavage at position 16 of insulin β-chain. Of note is the fact that z and y-NH$_3$ are isomeric as shown for $z16$ and y-16-NH$_3$.

NH$_3$ ions, and the $z'46$ and $z46$/$y46$-NH$_3$ ions, in MALDI-ISD FT-ICR MS spectra of a mAb heavy chain. From the figure, it becomes clear that such overlap between the different fragment ions resulted in an apparent increased relative signal intensity of the first three or four isotopologues of z' ions. This effect, with regard to the peak intensity of z' ions, was observed both

in mFT and aFT mass spectra, albeit aFT visualization helped resolve the overlapping species and thus increased confidence of the identifications.

Simulations of Different Ratios of z/y-NH$_3$ and z' Ions in MALDI-ISD Spectra. It will be obvious that the extent of overlap of z' and z/y-NH$_3$ ions depends on resolving power of

the mass measurement, and hence on the m/z of the fragment ions (as the resolution of ions in FTMS is a function of the m/z). To further investigate this, the overlap between z' and z/y-NH_3, at different relative intensity ratios, was simulated for the mAb heavy chain using the resolving powers that corresponded to mFT and aFT modes in the NIST mAb spectrum described above (Figures 3A,D). In the calculated mFT mass spectra, no deviations from the isotopic distributions were observed below ~m/z 1750 because all peaks were sufficiently resolved, whereas for larger z' ions, deviations (FoMs < 1) were clear (Figures 3B,E, S3, and S4).

Since the resolving power of FT-ICR mass spectra decreases at higher m/z-values (Figure S2), an increasing overlap can be observed between z/y-NH_3 and z', as the fragment sizes increase, with a consequent decrease of the FoM of the isotopic distribution of z' ions (Figure 3A,D). For example, the interference of $z46/y46$-NH_3 induced changes in both the mass accuracy and the relative peak height of $z'46$ isotopologues (Figures 3C,F and S5) as also observed in the measured mass spectrum (Figure 2). The FoM quality metric of the isotopic distribution of z' ions reaches a minimum at about m/z 4200 and increases again at higher m/z values due to the fact that the isotopic distributions turn broader (Figure S6). In the aFT mass spectra, some of the deviations were larger than in mFT spectra as a result of the additional overlap between negative side lobes and positive signals of aFT isotopic distributions (Figure S7).

This simulation does not account for the coalescence of peaks with small m/z differences which is a common process in FT-ICR MS.[45] Peak coalescence of two or more peaks with similar m/z values results in detection of a single peak even at theoretically sufficient resolving powers. Consequently, deviations in the isotopic distribution in measured spectra differ from the simulated deviations.

It is noted that the calculation of the FoM was solely based on peak intensities without accounting for the m/z shifts induced by the overlap between z/y-NH_3 and z' ions. In fact, the observed mass measurement errors of z' ions isotopologues were, on average, larger than those expected; thus, these were not included in the calculation of the quality of the isotopic distributions (Figure S8).

In MALDI-ISD FT-ICR MS spectra of proteins, z/y-NH_3 and z' are observed at different intensity ratios thus, the simulation was also performed considering different relative peak intensities of z/y-NH_3 ions (i.e., at 10%, 25%, 50%, and 75% the intensity of the z' ions). These simulations illustrate why higher deviations from the theoretical, pure isotopic distributions are expected when the ratio increases (Figures S4–S7).

In addition to theoretical deviations, other factors (e.g., overlap with other species, peak coalescence, space charge effect, see Figure 2) may also contribute to the distortion of the isotopic distribution, especially in complex spectra such as those obtained from top-down analysis of proteins where z' ions have low abundance.

The FoM values of the observed aFT distributions of $z'16$ and $z'46$ ions, depicted in Figure 2C,D, were 0.95 and 0.81, respectively. These values are in agreement with the theoretical FoM values reported in Figure 3. In fact, for $z16$ and $z'16$ ions, a theoretical FoM value of 1.0 was calculated at relative abundances (i.e., z/z') of 0.10 and 0.25 while, for $z46$ and $z'46$ ions, theoretical FoM values of 0.88 and 0.79 were calculated at relative abundances of 0.25 and 0.50, respectively. Observed

$z16/z'16$ and $z46/z'46$ were approximately 0.18 and 0.35. Thus, while the difference between FoM values of observed and theoretical distributions of $z'16$ ion can be explained considering other factors rather than the presence of $z16/y16$-NH_3 ions, the difference between FoM values of observed and theoretical distributions of $z'46$ ions are largely explained by the overlap with the isotopic distribution of $z46/y46$-NH_3 ions. This latter consideration allows increasing the confidence in the identification (and the assignment) of $z'46$ ion.

This evaluation clearly exemplifies that the presence of z/y-NH_3 affects the quality of MALDI-ISD FT-ICR MS spectra with an effect on the confidence of the assignment of z' ions and corroborates the observations in measured mass spectra such as those depicted in Figure 2.

Co-occurrence of z and y-NH_3 Ions in MALDI-ISD FT-ICR MS Spectra of Human Insulin. In MALDI-ISD FT-ICR MS spectra, the identity of fragment ions at 2.0157 mass units lower than the z' analogue can be either z or y-NH_3. To further study these two isomeric types of fragments, MALDI-ISD MS measurements were undertaken in which z and y-NH_3 ions contributed to the signal at various extents. For this, we applied two different. MALDI matrices which give slightly different MALDI-ISD MS profiles, indicating the activation of different fragmentation pathways. Alongside 1,5-DAN, we used N-phenyl-p-phenylenediamine (PPDA) as a matrix to generate ISD fragmentation profiles from human insulin (Figures S12–S14). A detailed comparison between the spectra obtained for the two different MALDI matrices is shown in Figure 4 for fragment ions detected in the m/z-range 1820–1980.

A large number of fragment ions from various classes were detected: namely a, b, c, d, w, Y, y, z', and z/y-NH_3 type. In general, the fragmentation pattern obtained using PPDA was similar to 1,5-DAN, with differences in the relative abundance of specific fragment ions such as z/y-NH_3 and z', Y and y, and b and d. The structures of C-terminal fragment ions generated from the cleavage at position 16 are reported in Figure 4C. Isomeric $z16$ and $y16$-NH_3 ions were detected at m/z 1876.9291 and 1876.9295, in the spectra obtained using 1,5-DAN and PPDA, respectively. The ratios between $z'16$ and $z16/y16$-NH_3, and between $y16$ and Y-16 were higher in mass spectra obtained using 1,5-DAN compared to PPDA. In addition to these differences, lower levels of reduction of the intrachain disulfide bond of insulin α chain fragments were observed in the spectrum generated using PPDA. For example, the $c17$ fragment of insulin α chain was detected with reduced cysteines at m/z 1887.8657 and with oxidized cysteines at m/z 1885.8486. The ratio between these fragment ions was higher for 1,5-DAN than for PPDA.

The intensity of z/y-NH_3 ions in the MALDI-ISD FT-ICR MS spectra was prominent and the ratio between z'- and z/y-NH_3 ions was dependent on the residue on the C-terminal side of the fragmentation site (see below). The co-occurrence of z and y-NH_3 ions in the spectra was corroborated by the following considerations and observations. As reported in Figure 1, z ions are formed from $z\bullet$, after the abstraction of one hydrogen from the β-carbon. Thus, z ions cannot be formed when a glycine is C-terminal to the cleavage site. This was further investigated in the MALDI-ISD FT-ICR MS spectra obtained from insulin that contains three glycine residues in the β-chain. In the resulting spectra, $z'11$ and $z'23$ ions, generated from the cleavage of the Cys7-Gly8 and the Cys19-Gly20 bonds, were detected at m/z 1287.6369 and m/z 2572.2876, respectively (Figure 5). Ion species were also
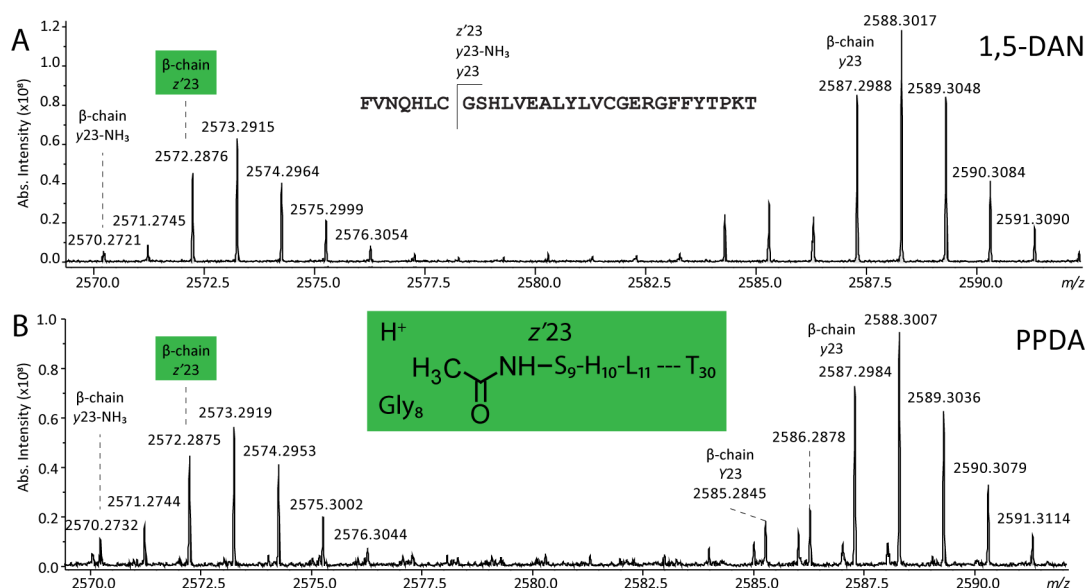
Figure 5. Evaluation of isomeric z and y-NH$_3$ fragment ions generated from glycine-8 C-terminal to the cleavage site in MALDI-ISD FT-ICR mass spectra of insulin analyzed using (A) 1,5-DAN and (B) PPDA. Since z ions cannot be formed from glycine residues (see scheme in Figure 1) the fragment ions detected at m/z 2570.2721 and m/z 2570.2732, in the two mass spectra, respectively, were identified as $y23$-NH$_3$ ions. The ratio between $y23$-NH$_3$ and $z'23$ was higher for PPDA than 1,5-DAN.

detected at m/z 1285.6204 and m/z 2570.2721; however, since z fragments cannot be generated from glycine C-terminal to the cleavage site, these signals can only be explained from a neutral loss of ammonia from $y11$ and $y23$ (detected at m/z 1302.6477 and m/z 2587.2988, respectively). The loss of ammonia from these y ions was more pronounced in the spectra generated with PPDA than 1,5-DAN (Figure 5).

The relative abundance of z/y-NH$_3$, z', and y ions was evaluated for each cleavage site. To this end, the intensity of each z/y-NH$_3$ and y ion of insulin β-chain was normalized on the intensity of the corresponding z' ion and plotted against the amino acid residue C-terminal to the cleavage site (Figure S15). As shown above for the heavy chain of NIST mAb, also for insulin β-chain, the relative intensity of z/y-NH$_3$ and z' ions was found to be dependent on the amino acid residue C-terminal to the cleavage site. On average, the lowest and highest ratios (i.e., 0.10 and 0.94) were found for glycine and valine residues, respectively.

Discerning z and y-NH$_3$ Fragmentation in MALDI-ISD Using Synthetic Peptides. The observation of z/y-NH$_3$ signal for peptides with glycine residues C-terminal to the cleavage sites confirmed the presence of y-NH$_3$ ions in MALDI-ISD FT-ICR MS of proteins. In order to demonstrate the opposite, namely formation of z-ions, a pair of synthetic peptides was characterized, both with the sequence EAGA-GAGARERWNKALEPAK, but where the alanine residues (at position 2, 4, 6, and 8) in one of the peptides had a deuterated methyl group (β-carbon). The MALDI-ISD FT-ICR MS spectra obtained from the analysis of these peptides are reported in Figure S16.

The use of 1,5-DAN allowed an extensive fragmentation of the synthetic peptides, while ultrahigh resolution FT-ICR MS allowed a confident assignment of the fragment ions in the spectra. Figure 6A,B shows the observed isotopic distributions of fragment ions with light and heavy Ala6, C-terminal to the cleavage site. The $z15'$ fragment ions, generated from the light and the heavy peptides, were observed at m/z 1681.9145 and 1687.9515, respectively.

The abstraction of one hydrogen atom from light Ala6 and one deuterium from heavy Ala6 generated $z15\bullet$-H and $z15\bullet$-D fragment ions which were detected at m/z 1679.8976 and m/z 1684.9307, respectively. Interestingly, differences were observed between the theoretical and the observed isotopic distribution of $z15\bullet$-D (i.e., a different isotopic peak being the most intense) indicating the co-occurrence of z and y-NH$_3$ ions. Such differences were larger in the MALDI-ISD FT-ICR MS spectrum obtained using PPDA (Figure 6C).

The higher degree of loss of ammonia in the mass spectrum obtained using PPDA was also observed at intact protein level. In fact, for the heavy peptide, the intensity of $[M-NH_3+H]^+$ was 2% of the signal of $[M + H]^+$ for 1,5-DAN and 9% for PPDA. It is commonly assumed that loss of ammonia occurs from arginine, lysine, glutamate, and asparagine residues upon vibrational activation. Thus, we assumed that a loss of ammonia involving the abstraction of one deuterium from heavy Ala6 is unlikely and that the signal observed at m/z 1684.9307 derived solely from $z15\bullet$-D.

Similar results, with regard to the abstraction of either one hydrogen atom or deuterium, were obtained for the fragments with Ala2 and Ala4 (Figures S17 and S18) C-terminal to the cleavage site. The analysis of fragments from Ala8 was affected by unresolved fragment ions (i.e., $y13$-NH$_3$ of m/z 1554.8578 and $c15$ of m/z 1554.8637).

The observations in insulin and synthetic peptides corroborate the hypothesis that z and y-NH$_3$ fragmentations co-occur during radical-mediated MALDI-ISD of proteins. It is however noted that a generalized conclusion on the structural factors (e.g., residues N- and C-terminal to the cleavage site and presence of Arg, Lys, Asn, and Gln) that steer ISD fragmentation toward z or y-NH$_3$ requires evaluation of a large number of peptides.

◼ CONCLUSIONS

In this study, we showed that the detected isotopic distribution of z' fragment ions, generated by MALDI-ISD FT-ICR MS of
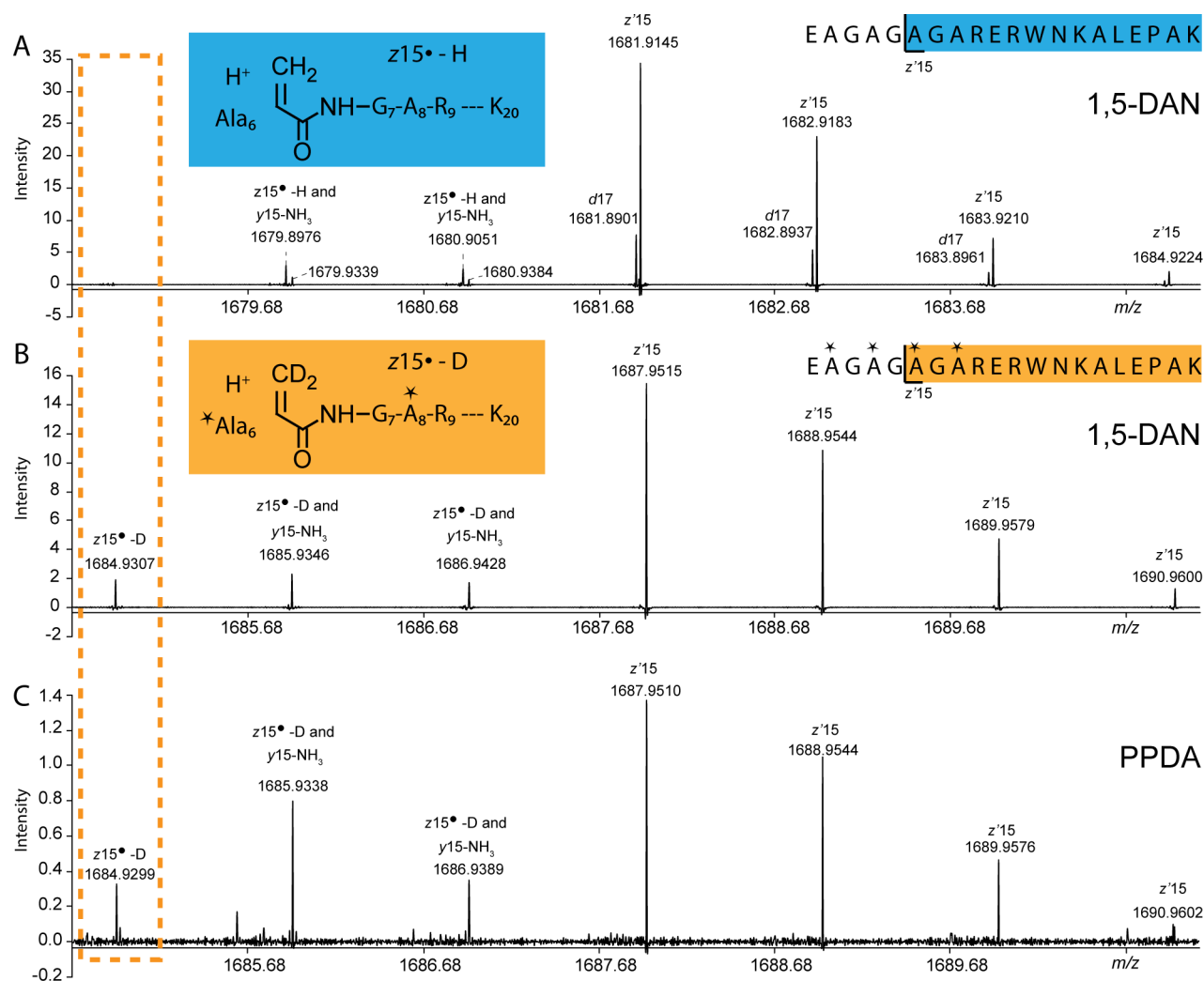
Figure 6. Evaluation of isomeric z and y-NH_3 ions in MALDI-ISD FT-ICR mass spectra obtained from the analysis of a pair of peptides, (A) one with normal alanine (m/z 2082.0814) analyzed with 1,5-DAN and one with heavy alanine (m/z 2094.1591) analyzed with both (B) 1,5-DAN and (C) PPDA. The abstraction of one deuterium instead of one hydrogen from alanine-6 led to the detection of an additional peak at m/z 1684.9307 (or m/z 1684.9299). The isotopic distribution on $z15^*$-D resulted distorted as a consequence of the presence of $y15$-NH_3 ions. Such a distortion was higher for PPDA than 1,5-DAN.

proteins (i.e., NIST mAb heavy chain), can be affected by the presence of interfering z and y-NH_3 fragment ion isotopic distributions. The z and y-NH_3 fragment ions are isomeric but are generated by different fragmentation paths.

A theoretical simulation of the overlap between the isotopic distributions of the z' and z/y-NH_3 ions showed the dependence of the signal distortion of z' ions with the resolving power, m/z values and relative intensity of the ions, in agreement with the observations in the measured mass spectra.

Co-occurrence of z and y-NH_3 fragment ions was evaluated by comparing MALDI-ISD FT-ICR mass spectra of insulin obtained from two matrices, namely 1,5-DAN and PPDA. This latter compound was used, for the first time, as a reducing MALDI-ISD matrix and yielded fragmentation spectra similar but not identical to those from 1,5-DAN. Cleavages C-terminal to glycine resulted only in the generation of y-NH_3 fragments. In contrast, for all other amino acids both y-NH_3 ions and z ions can be generated. To resolve the contribution of these isomeric y-NH_3 ions and z ions to MALDI-ISD MS spectra, peptides containing alanine residues with and without

perdeuterated methyl groups; as for the alanines with perdeuterated methyl groups, the y-NH_3 ions and z ions would differ in mass by ~1 Da and hence would be distinguishable in the mass spectra—were analyzed using both 1,5-DAN and PPDA.

We demonstrated that the relative abundance of z/y-NH_3 ions depends on the amino acid residue C-terminal to the cleaved peptide bond and that these ions can reach intensities similar to those of z' ions. Therefore, we conclude that co-occurring z/y-NH_3 ions in MALDI-ISD spectra of proteins can considerably contribute to the distortions of the isotopic distribution of z' ions. Consequently, the evaluation of their presence increases the confidence of the identifications and explains decreased FoM values of certain z' ions. This is of importance for detailed and accurate structural characterization of pharmaceutical products such as therapeutic mAbs. Here, confident identifications of fragment ions result in a more reliable structural characterization of the protein product.

In this study, we have reported on the formation of z/y-NH_3 ions in MALDI-ISD FT-ICR MS. Since fragmentation pathways and resulting products in MALDI-ISD are partly

influenced by the pressure of the MALDI ion source,[69,71,72] further research is warranted to elucidate the formation mechanism of z/y-NH_3 ions in different types of MALDI MS systems. This could lead to more sensitive MALDI-ISD MS methods where the generation of z/y-NH_3 ions is reduced in favor of more intense z' ions.

■ ASSOCIATED CONTENT

ⓈⒾ Supporting Information

The Supporting Information is available free of charge at https://pubs.acs.org/doi/10.1021/acs.analchem.9b05683.

Additional experimental details and supporting figures (PDF)

■ AUTHOR INFORMATION

Corresponding Author

Simone Nicolardi − *Center for Proteomics & Metabolomics, Leiden University Medical Center, Leiden 2333, ZA, The Netherlands;* ⓞ orcid.org/0000-0001-8393-1625; Email: s.nicolardi@lumc.nl

Authors

David P. A. Kilgour − *Department of Chemistry, Nottingham Trent University, Nottingham NG11 0JN, United Kingdom*

Natasja Dolezal − *Department of Immunohematology and Blood Transfusion, Leiden University Medical Center, Leiden 2333, ZA, The Netherlands*

Jan W. Drijfhout − *Department of Immunohematology and Blood Transfusion, Leiden University Medical Center, Leiden 2333, ZA, The Netherlands*

Manfred Wuhrer − *Center for Proteomics & Metabolomics, Leiden University Medical Center, Leiden 2333, ZA, The Netherlands;* ⓞ orcid.org/0000-0002-0814-4995

Yuri E. M. van der Burgt − *Center for Proteomics & Metabolomics, Leiden University Medical Center, Leiden 2333, ZA, The Netherlands;* ⓞ orcid.org/0000-0003-0556-5564

Complete contact information is available at:
https://pubs.acs.org/10.1021/acs.analchem.9b05683

Notes

The authors declare no competing financial interest.

■ ACKNOWLEDGMENTS

■ REFERENCES

(1) Sleno, L.; Volmer, D. A. *J. Mass Spectrom.* **2004**, *39* (10), 1091−1112.

(2) Loo, J.; Edmonds, C.; Smith, R. *Science* **1990**, *248* (4952), 201−204.

(3) Kelleher, N. L.; Lin, H. Y.; Valaskovic, G. A.; Aaserud, D. J.; Fridriksson, E. K.; McLafferty, F. W. *J. Am. Chem. Soc.* **1999**, *121* (4), 806−812.

(4) Zhang, Y.; Fonslow, B. R.; Shan, B.; Baek, M.-C.; Yates, J. R. *Chem. Rev.* **2013**, *113* (4), 2343−2394.

(5) Brodbelt, J. S. *Anal. Chem.* **2016**, *88* (1), 30−51.

(6) Dongré, A. R.; Jones, J. L.; Somogyi, Á.; Wysocki, V. H. *J. Am. Chem. Soc.* **1996**, *118* (35), 8365−8374.

(7) Tureček, F.; Julian, R. R. *Chem. Rev.* **2013**, *113* (8), 6691−6733.

(8) Zubarev, R. A.; Kelleher, N. L.; McLafferty, F. W. *J. Am. Chem. Soc.* **1998**, *120* (13), 3265−3266.

(9) Macias, L. A.; Santos, I. C.; Brodbelt, J. S. *Anal. Chem.* **2020**, *92*, 227.

(10) Roepstorff, P.; Fohlman, J. *Biomed. Mass Spectrom.* **1984**, *11* (11), 601.

(11) Biemann, K. *Biol. Mass Spectrom.* **1988**, *16* (1−12), 99−111.

(12) Biemann, K. *Methods Enzymol.* **1990**, *193*, 886−7.

(13) Steen, H.; Mann, M. *Nat. Rev. Mol. Cell Biol.* **2004**, *5* (9), 699−711.

(14) Asakawa, D. *J. Am. Soc. Mass Spectrom.* **2019**, *30* (8), 1491−1502.

(15) Fälth, M.; Savitski, M. M.; Nielsen, M. L.; Kjeldsen, F.; Andren, P. E.; Zubarev, R. A. *Anal. Chem.* **2008**, *80* (21), 8089−8094.

(16) Xia, Q.; Lee, M. V.; Rose, C. M.; Marsh, A. J.; Hubler, S. L.; Wenger, C. D.; Coon, J. J. *J. Am. Soc. Mass Spectrom.* **2011**, *22* (2), 255−264.

(17) Lermyte, F.; Valkenborg, D.; Loo, J. A.; Sobott, F. *Mass Spectrom. Rev.* **2018**, *37* (6), 750−771.

(18) Mitchell Wells, J.; McLuckey, S. A. Collision-Induced Dissociation (CID) of Peptides and Proteins. *Methods Enzymol.*; Academic Press: New York, 2005; Vol. *402*, pp 148−185.

(19) Syka, J. E.; Coon, J. J.; Schroeder, M. J.; Shabanowitz, J.; Hunt, D. F. *Proc. Natl. Acad. Sci. U. S. A.* **2004**, *101* (26), 9528−33.

(20) Ge, Y.; Lawhorn, B. G.; ElNaggar, M.; Strauss, E.; Park, J.-H.; Begley, T. P.; McLafferty, F. W. *J. Am. Chem. Soc.* **2002**, *124* (4), 672−678.

(21) Brodbelt, J. S. *Chem. Soc. Rev.* **2014**, *43* (8), 2757−2783.

(22) Shaw, J. B.; Li, W.; Holden, D. D.; Zhang, Y.; Griep-Raming, J.; Fellers, R. T.; Early, B. P.; Thomas, P. M.; Kelleher, N. L.; Brodbelt, J. S. *J. Am. Chem. Soc.* **2013**, *135* (34), 12646−51.

(23) Cammarata, M. B.; Thyer, R.; Rosenberg, J.; Ellington, A.; Brodbelt, J. S. *J. Am. Chem. Soc.* **2015**, *137* (28), 9128−9135.

(24) Riley, N. M.; Westphall, M. S.; Coon, J. J. *J. Proteome Res.* **2017**, *16* (7), 2653−2659.

(25) Tran, J. C.; Zamdborg, L.; Ahlf, D. R.; Lee, J. E.; Catherman, A. D.; Durbin, K. R.; Tipton, J. D.; Vellaichamy, A.; Kellie, J. F.; Li, M. X.; Wu, C.; Sweet, S. M. M.; Early, B. P.; Siuti, N.; LeDuc, R. D.; Compton, P. D.; Thomas, P. M.; Kelleher, N. L. *Nature* **2011**, *480* (7376), 254−U141.

(26) Chaurand, P.; Luetzenkirchen, F.; Spengler, B. *J. Am. Soc. Mass Spectrom.* **1999**, *10* (2), 91−103.

(27) Andersen, J. S.; Svensson, B.; Roepstorff, P. *Nat. Biotechnol.* **1996**, *14* (4), 449−457.

(28) Kocher, T.; Engstrom, A.; Zubarev, R. A. *Anal. Chem.* **2005**, *77* (1), 172−177.

(29) Hardouin, J. *Mass Spectrom. Rev.* **2007**, *26* (5), 672−682.

(30) Takayama, M. *Mass Spectrom.* **2016**, *5* (1), A0044−A0044.

(31) Demeure, K.; Quinton, L.; Gabelica, V.; De Pauw, E. *Anal. Chem.* **2007**, *79* (22), 8678−8685.

(32) Asakawa, D.; Sakakura, M.; Takayama, M. *Mass Spectrom.* **2012**, *1* (1), A0002.

(33) Brown, R. S.; Carr, B. L.; Lennon, J. J. *J. Am. Soc. Mass Spectrom.* **1996**, *7* (3), 225−232.

(34) Fukuyama, Y.; Iwamoto, S.; Tanaka, K. *J. Mass Spectrom.* **2006**, *41* (2), 191−201.

(35) Demeure, K.; Gabelica, V.; De Pauw, E. A. *J. Am. Soc. Mass Spectrom.* **2010**, *21* (11), 1906−1917.

(36) Asakawa, D.; Smargiasso, N.; De Pauw, E. *J. Am. Soc. Mass Spectrom.* **2013**, *24* (2), 297−300.

(37) Asakawa, D.; Smargiasso, N.; De Pauw, E. *Anal. Chem.* **2014**, *86* (5), 2451−2457.

(38) Nicolardi, S.; Switzar, L.; Deelder, A. M.; Palmblad, M.; van der Burgt, Y. E. M. *Anal. Chem.* **2015**, *87* (6), 3429−3437.

(39) van der Burgt, Y. E. M.; Kilgour, D. P. A.; Tsybin, Y. O.; Srzentić, K.; Fornelli, L.; Beck, A.; Wuhrer, M.; Nicolardi, S. *Anal. Chem.* **2019**, *91* (3), 2079−2085.

(40) Yu, X.; Sargaeva, N. P.; Thompson, C. J.; Costello, C. E.; Lin, C. *Int. J. Mass Spectrom.* **2015**, *390*, 101−109.

(41) Asakawa, D.; Calligaris, D.; Smargiasso, N.; De Pauw, E. *J. Phys. Chem. B* **2013**, *117* (8), 2321–2327.

(42) Tyshchuk, O.; Gstöttner, C.; Funk, D.; Nicolardi, S.; Frost, S.; Klostermann, S.; Becker, T.; Jolkver, E.; Schumacher, F.; Koller, C. F.; Völger, H. R.; Wuhrer, M.; Bulau, P.; Mølhøj, M. *mAbs* **2019**, *11* (7), 1219–1232.

(43) Dilillo, M.; de Graaf, E. L.; Yadav, A.; Belov, M. E.; McDonnell, L. A. *J. Proteome Res.* **2018**, *18* (1), 557–564.

(44) Nicolardi, S.; van der Burgt, Y. E. M.; Codée, J. D. C.; Wuhrer, M.; Hokke, C. H.; Chiodo, F. *ACS Nano* **2017**, *11* (8), 8257–8264.

(45) Boldin, I. A.; Nikolaev, E. N. *Rapid Commun. Mass Spectrom.* **2009**, *23* (19), 3213–9.

(46) Mathur, R.; O'Connor, P. B. *Rapid Commun. Mass Spectrom.* **2009**, *23* (4), 523–529.

(47) Vladimirov, G.; Hendrickson, C. L.; Blakney, G. T.; Marshall, A. G.; Heeren, R. M. A.; Nikolaev, E. N. *J. Am. Soc. Mass Spectrom.* **2012**, *23* (2), 375–384.

(48) Dittwald, P.; Valkenborg, D.; Claesen, J.; Rockwood, A. L.; Gambin, A. *J. Am. Soc. Mass Spectrom.* **2015**, *26* (10), 1732–1745.

(49) Nikolaev, E. N.; Kostyukevich, Y. I.; Vladimirov, G. N. *Mass Spectrom. Rev.* **2016**, *35* (2), 219–58.

(50) Savitski, M. M.; Kjeldsen, F.; Nielsen, M. L.; Zubarev, R. A. *J. Am. Soc. Mass Spectrom.* **2007**, *18* (1), 113–20.

(51) Hamidane, H. B.; Chiappe, D.; Hartmer, R.; Vorobyev, A.; Moniatte, M.; Tsybin, Y. O. *J. Am. Soc. Mass Spectrom.* **2009**, *20* (4), 567–575.

(52) Zubarev, R. A.; Horn, D. M.; Fridriksson, E. K.; Kelleher, N. L.; Kruger, N. A.; Lewis, M. A.; Carpenter, B. K.; McLafferty, F. W. *Anal. Chem.* **2000**, *72* (3), 563–573.

(53) Asakawa, D.; Smargiasso, N.; Quinton, L.; De Pauw, E. *J. Am. Soc. Mass Spectrom.* **2014**, *25* (6), 1040–1048.

(54) Asakawa, D.; Takahashi, H.; Iwamoto, S.; Tanaka, K. *Phys. Chem. Chem. Phys.* **2018**, *20* (18), 13057–13067.

(55) van der Rest, G.; Hui, R.; Frison, G.; Chamot-Rooke, J. *J. Am. Soc. Mass Spectrom.* **2011**, *22* (9), 1631–1644.

(56) Tureček, F.; Chung, T. W.; Moss, C. L.; Wyer, J. A.; Ehlerding, A.; Holm, A. I. S.; Zettergren, H.; Nielsen, S. B.; Hvelplund, P.; Chamot-Rooke, J.; Bythell, B.; Paizs, B. *J. Am. Chem. Soc.* **2010**, *132* (31), 10728–10740.

(57) Zhang, Z. *Anal. Chem.* **2010**, *82* (5), 1990–2005.

(58) Hamidane, H. B.; He, H.; Tsybin, O. Y.; Emmett, M. R.; Hendrickson, C. L.; Marshall, A. G.; Tsybin, Y. O. *J. Am. Soc. Mass Spectrom.* **2009**, *20* (6), 1182–1192.

(59) Srzentic, K.; et al. Consortium for Top-Down Proteomics Inter-laboratory Study for Characterizing Monoclonal Antibodies (mAbs) by Top-Down Mass Spectrometry. *66th ASMS Conference on Mass Spectrometry and Allied Topics 2018 San Diego* **2018**, Poster ID 294106.

(60) Hiemstra, H. S.; Duinkerken, G.; Benckhuijsen, W. E.; Amons, R.; de Vries, R. R. P.; Roep, B. O.; Drijfhout, J. W. *Proc. Natl. Acad. Sci. U. S. A.* **1997**, *94* (19), 10313–10318.

(61) Kilgour, D. P. A.; Wills, R.; Qi, Y.; O'Connor, P. B. *Anal. Chem.* **2013**, *85* (8), 3903–3911.

(62) Kilgour, D. P.; Neal, M. J.; Soulby, A. J.; O'Connor, P. B. *Rapid Commun. Mass Spectrom.* **2013**, *27* (17), 1977–82.

(63) Kilgour, D. P.; Van Orden, S. L. *Rapid Commun. Mass Spectrom.* **2015**, *29* (11), 1009–18.

(64) Kilgour, D. P. A.; Hughes, S.; Kilgour, S. L.; Mackay, C. L.; Palmblad, M.; Tran, B. Q.; Goo, Y. A.; Ernst, R. K.; Clarke, D. J.; Goodlett, D. R. *J. Am. Soc. Mass Spectrom.* **2017**, *28* (2), 253–262.

(65) Rockwood, A. L.; Van Orden, S. L.; Smith, R. D. *Anal. Chem.* **1995**, *67* (15), 2699–2704.

(66) Rockwood, A. L.; Van Orden, S. L. *Anal. Chem.* **1996**, *68* (13), 2027–30.

(67) Kilgour, D. P.; Van Orden, S. L.; Tran, B. Q.; Goo, Y. A.; Goodlett, D. R. *Anal. Chem.* **2015**, *87* (11), 5797–801.

(68) Strohalm, M.; Hassman, M.; Košata, B.; Kodíček, M. *Rapid Commun. Mass Spectrom.* **2008**, *22* (6), 905–908.

(69) Asakawa, D.; Calligaris, D.; Zimmerman, T. A.; Pauw, E. D. *Anal. Chem.* **2013**, *85* (16), 7809–7817.

(70) Gstöttner, C.; Reusch, D.; Haberger, M.; Dragan, I.; van Veelen, P.; Kilgour, D. P. A.; Tsybin, Y. O.; van der Burgt, Y. E. M.; Wuhrer, M.; Nicolardi, S. *mAbs* **2020**, *12*, 1682403.

(71) Soltwisch, J.; Souady, J.; Berkenkamp, S.; Dreisewerd, K. *Anal. Chem.* **2009**, *81* (8), 2921–2934.

(72) Soltwisch, J.; Dreisewerd, K. *Anal. Chem.* **2010**, *82* (13), 5628–5635.